ELSEVIER

Dynamics of Atmospheres and Oceans 23 (1996) 321–334

dynamics of atmospheres and oceans

Stratified flow over three-dimensional topography

Y. Kadri [a], P. Bonneton [b], J.M. Chomaz [c], M. Perrier [a,*]

[a] *METEO-FRANCE, 42 avenue Coriolis, 31057 Toulouse, France*

[b] *Institut de Mecanique des Fluides de Toulouse (IMFT), avenue du Professeur Camille Soula, 31400 Toulouse, France*

[c] *Laboratoire d'Hydrodynamique (LADHYX), Ecole Polytechnique, 91128 Palaiseau-Cedex, France*

Received 12 September 1994; revised 2 February 1995; accepted 9 March 1995

Abstract

In order to investigate flows over topography in an atmospheric context, we have studied experimentally the wake structure of axi-symmetric Gaussian obstacles towed through a linearly stratified fluid. Three dimensionless parameters govern the flow dynamics: F, the Froude number based on the topography height h; Re, the Reynolds number and the aspect ratio $r = h/L$, where L is the topography horizontal scale. Two-dimensional (2-D), saturated lee wave (SLW) and three-dimensional (3-D) regimes, as defined in Chomaz et al. (1993), are found to be functions of F and r only (Fig. 1) as soon as Re is larger than $\mathrm{Re}_c \approx 2000$. For $F < 0.7$ the flow goes around the obstacle and the motion in the wake is quasi-two-dimensional. This 2-D layer is topped by a region affected by lee wave motions with amplitude increasing with r and F. For $0.7 < F < 1/r$, the flow is entirely dominated by a lee wave of saturated amplitude which suppresses the separation of the boundary layer from the obstacle. Above the critical value $1/r$, the lee wave amplitude decreases with F and a recirculating zone appears behind the obstacle. Simultaneously, coherent large-scale vortices start to be shed periodically from the wake at a Strouhal number which decreases as $1/F$ until it reaches its neutral asymptotic value.

1. Introduction

Recently, a large research effort has been devoted to the study of geophysical flows over topography. Such phenomena are particularly important in meteorological or oceanographic contexts, since the Earth's topographies generate internal gravity waves that transfer energy from the bottom layers to the upper layers. The

* Corresponding author.

0377-0265/96/$15.00 © 1996 Elsevier Science B.V. All rights reserved
SSDI 0377-0265(95)00433-5

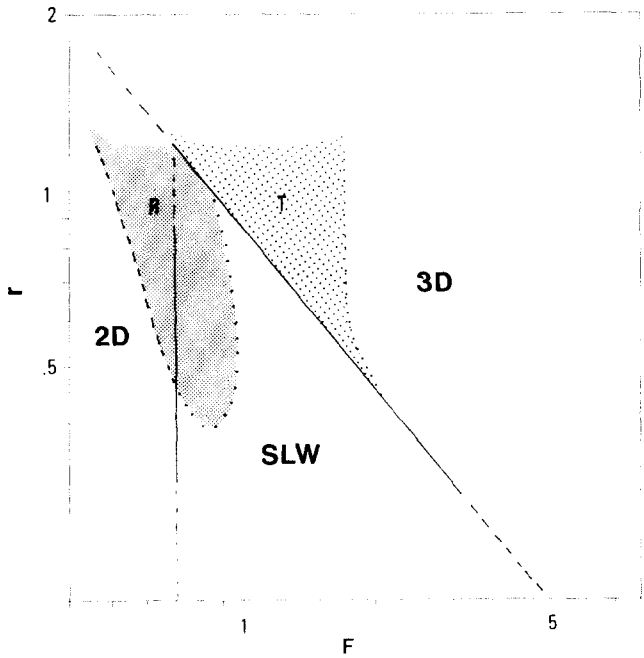

Fig. 1. Flow regime diagram (F, r): 2D, quasi-two-dimensional wake regime; SLW, 'saturated' lee wave regime (R, roller regime); 3D, three-dimensional wake regime (T, transition regime).

processes induced by the propagation of internal waves are important and ought to be taken into account in weather forecasting models. New developments of non-hydrostatic models require precise laboratory experiments in order to document test cases. Brighton (1978) and Hunt and Snyder (1980), studying reliefs with aspect ratios ($r = h/L$) close to 1, have shown that such flows are mainly controlled by the Froude number $F = U/Nh$, where U is the flow velocity and N is the Brunt–Väisälä frequency of the medium. They demonstrated that for small values of F, the near wake is quasi-two-dimensional, and that for $F \approx 1$, the flow separation line is conditioned by the lee wave. Chomaz et al. (1992, 1993) and Lin et al. (1992) have extended such an investigation by examining the dynamics of the stratified flow past a sphere for large ranges of Froude and Reynolds numbers. Theoretical analyses of stratified flow over a three-dimensional (3-D) obstacle have been elaborated by Smith (1980, 1989), for the hydrostatic framework, and by Crapper (1959), Lighthill (1978) and Voisin (1994) for the non-hydrostatic approach. In this paper we describe the near wake structure of axi-symmetric Gaussian obstacles towed in a linearly stratified fluid. We demonstrate the influence of both the Froude number and the aspect ratio, on the flow structure (Fig. 1).

Experiments were performed in a water towing tank of size $0.5 \times 0.5 \times 4$ m^3. This tank was filled with a linear stratification using salt solutions $N \in [0.67, 2$ rad s$^{-1}]$. Four Gaussian models were used in the experiments $r \in [0.28, 0.56, 0.8, 1.12]$.

The Gaussian obstacle was suspended by five stainless steel wires, of 0.1 mm in diameter, and was towed along the bottom of the tank. The towing velocity varied from 0.5 to 25 cm s^{-1}. When, for a given stratification N and a given model r, the velocity is varied, the two dimensionless numbers F and Re (Re $= U(2L)/\nu$, where ν is the kinematic viscosity), evolve proportionally in the form $\mathrm{Re}(F) = \mathrm{Re}(1)F$, where $\mathrm{Re}(1) = 2rNL^2/\nu$. In the present study, F was varied from 0.2 to 14 and Re from 300 to 25 000. Visualization and measurement techniques used in the experiments have been described in detail in Bonneton et al. (1993) and Chomaz et al. (1993).

2. The lee wave dynamics

Particle streak photographs of the flow over two Gaussian models $r = 0.28$ (Figs. 2(a)–(c)) and $r = 0.8$ (Figs. 2(d)–(f)) illustrate the evolution of the lee wave structure as a function of F. At large F (Figs. 2(a) and (d)) a 3-D recirculating zone is present behind the obstacles (3-D regime in Fig. 1). Both the size and the unsteadiness of this zone increase with F, whereas the lee wave amplitude decreases. For weaker F (Figs. 2(b) and (e)) the flow is entirely dominated by a saturated lee wave which suppresses the turbulent wake (SLW regime in Fig. 1). For F smaller than 0.7 (Figs. 2(c) and (f)), the lee wave amplitude decreases and a 2-D layer appears close to the ground (2-D regime in Fig. 1). For $r = 0.28$ (Fig. 2(c)) the wave amplitude is much smaller than for $r = 0.8$ (Fig. 2(f)) and only the first crest is visible. The lee wave wavelengths measured from these visualizations are in good agreement with the theoretical law ($\lambda = 2\pi U/N$), even for small F, and with no significant influence from the body shape.

From particle tracking we have determined the spatial distribution of the vertical component of the velocity field (see Fig. 3(a)), which enables us to deduce the distribution of the local amplitude of the lee wave. In Fig. 3(b), we have shown for $r = 0.28$ and $r = 0.8$, the angle θ between the horizontal and the direction where the local wave amplitude is maximum. We can see that for both models, θ decreases notably between $F \approx 1.2$ and 1.6. Even if the precision is rather poor for $r = 0.28$ when F is close to 0.4, because of the small amplitude of the lee wave, Fig. 3(b) clearly demonstrates that θ is much larger for $r = 0.28$ than for $r = 0.8$. For small values of r and F, the measured angle θ is close to the theoretical value 90° obtained with the hydrostatic approximation. However, we note that even for $r = 0.28$, the lee wave dynamics do not correspond totally to hydrostatic behaviour, with horizontal isophases and, in the obstacle frame, a vertical propagation of wave energy. Fig. 4 presents the evolution of the maximum vertical displacement ζ of a fluid particle, owing to the lee wave, as a function of F for $r = 0.28$ and $r = 0.8$. For both cases, we observe that the amplitude (ζ/h) increases until F reaches 0.7 (2-D regime). Then, it saturates around $F \approx 1$ (SLW regime) and finally, starts to decrease for F larger than $1/r$. Similar behaviour is obtained for the two other models $r = 0.56$ and $r = 1.12$. The initial increase of the amplitude with F may be explained by the energetic arguments of Sheppard (1956) which predict: $\zeta/h = F$.

However, the theoretical predictions seem to overestimate the amplitude for the small aspect ratio ($r = 0.28$) and underestimate it for large r ($r = 0.8$). The transition in the lee wave amplitude for $F \approx 1/r$, has been theoretically predicted

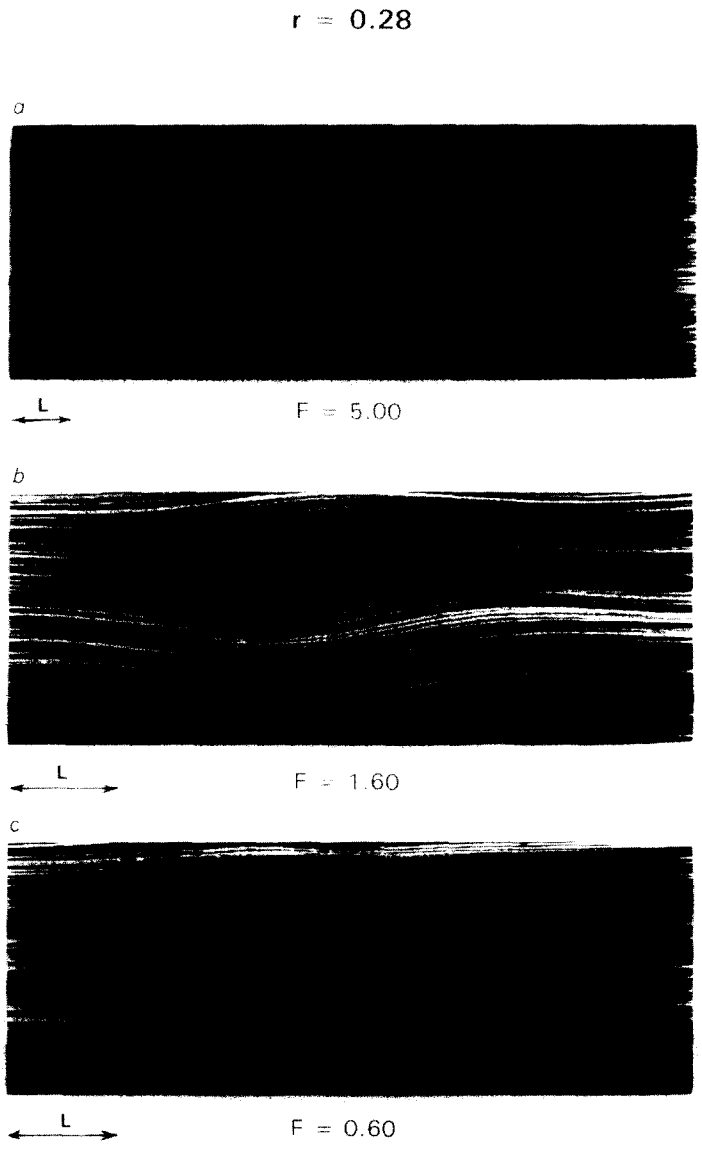

Fig. 2. Particle streak trajectories in the vertical central plane, for $r = 0.28$ (Re(1) = 1600) and for $r = 0.8$ (Re(1) = 2100). (The flow is from left to right on all figures).

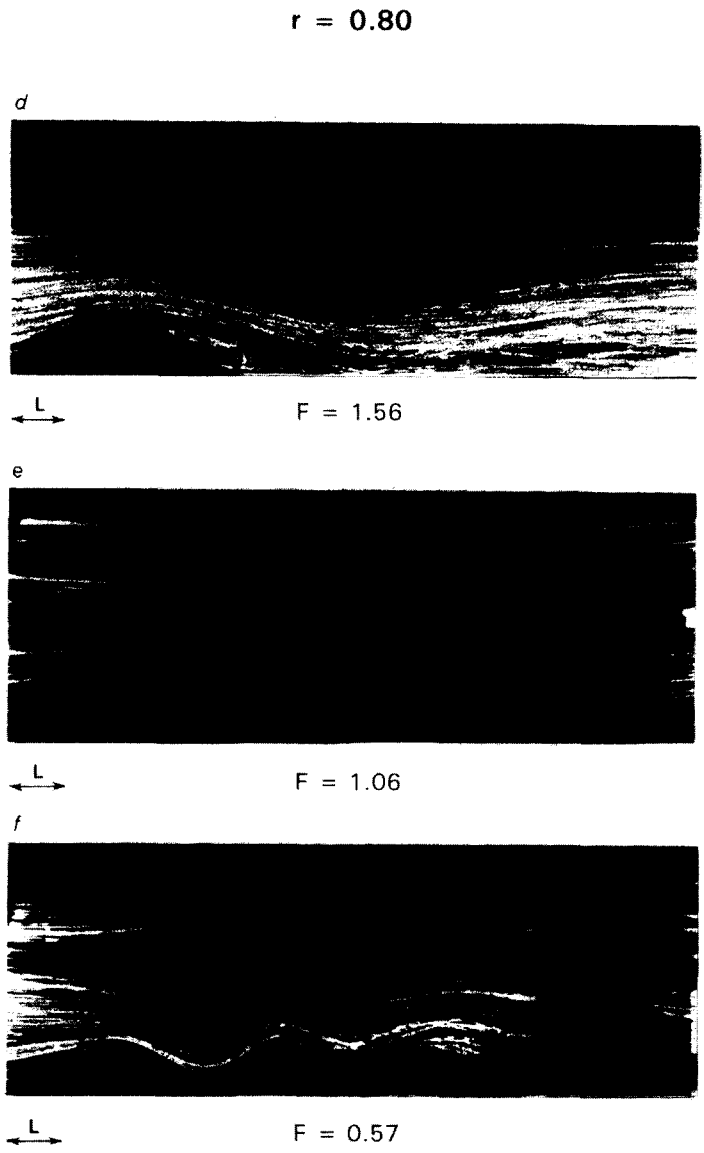

Fig. 2 (continued).

by Queney (1948) who argued that a resonant regime occurs when the effective wavelength of the mountain ($2\pi L$) equals the lee wave wavelength ($2\pi U/N$). For $r = 0.8$, the decrease in amplitude observed at large F, seems to agree with the linear theory (Voisin, 1994) which predicts: $\zeta/h \approx 1/F$.

3. The three-dimensional wake regime ($F \geqslant 1/r$)

3.1. Homogeneous wake

In order to understand the stratification effects on the close wake ($Nt < 2.5$), knowledge of the wake in a homogeneous medium is required. As for the sphere (Kim and Durbin, 1988; Chomaz et al., 1993), we have observed that, for Reynolds numbers greater than a critical value Re_c, the wake is affected by two instability

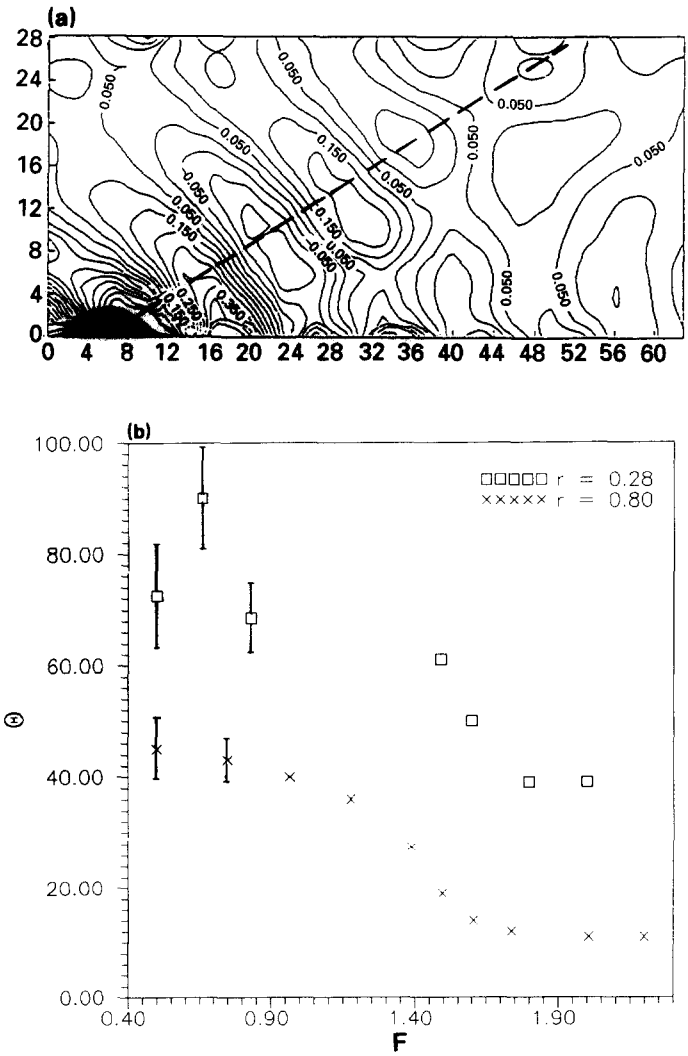

Fig. 3. (a) Vertical velocity field in the vertical central plane for $F = 0.97$ and $r = 0.8$ (Re(1) = 2100). (b) Evolution of the angle between the horizontal and the direction of maximum local vertical velocity versus F for $r = 0.28$ (Re(1) = 900) and for $r = 0.8$ (Re(1) = 2100).

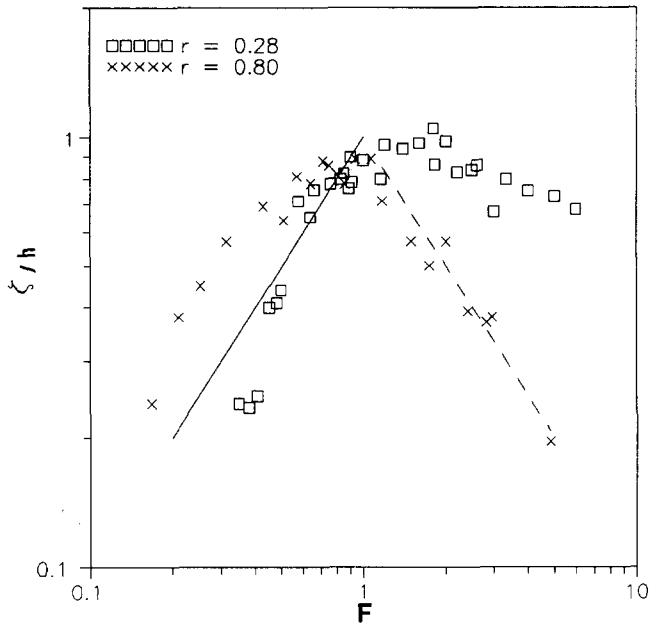

Fig. 4. Evolution of the wave amplitude versus F for $r = 0.28$ (Re(1) = 900, 1600 and 2400); and for $r = 0.8$ (Re(1) = 1300, 2100 and 2700). Continuous line, Sheppard's theory; dashed line, linear theory.

modes: a high-frequency Kelvin–Helmholtz shear instability (KH) of the separated layer and a low-frequency mode (VS) associated with the shedding of large-scale coherent vortices (Figs. 5(a) and (d)). For smaller Reynolds number values, only a single mode is present. Fig. 6 shows for $r = 0.8$, the evolution of the Strouhal numbers S ($S = f(2L)/U$, where f is the vortex shedding frequency), as obtained either from fluorescent dye visualizations (for low to moderate Re) or from the spectral analysis of hot film probe signals (for moderate to high Re). Above $\mathrm{Re}_c \approx 1300$, the Strouhal number of the low-frequency wake instability stabilises around $S_{vs} \approx 0.55$ whereas the high-frequency branch (KH mode) keeps increasing. Similar behaviour is observed for the different models tested, excepted that the power of the power-law fit of the KH Strouhal number versus Re, decreases with r. Values of Re_c and S_{vs} as a function of r are reported in Table 1.

3.2. Stratified wake

Fig. 5 illustrates the disappearance of the shedding of large- scale vortices as the stratification effects increase (F decreases). This phenomenon occurs at a critical Froude number F_c depending only on r as soon as $\mathrm{Re} > \mathrm{Re}_c$. For $r = 0.28$, F_c is close to 4 (Figs. 5(b) and (c)) whereas it is close to 1.2 for $r = 0.8$ (Figs. 5(e) and (f)). In Fig. 7 we have reported the evolution of the Strouhal number S of the VS instability as a function of rF for several aspect ratios ($r = 0.28$, 0.8 and 1.12).

Values of S were obtained either from visualizations or from both conductivity and velocity measurements. We note, from Fig. 7, that S decreases with F following an $1/rF$ law (transition regime T in Fig. 1) before stabilising at its neutral value. This

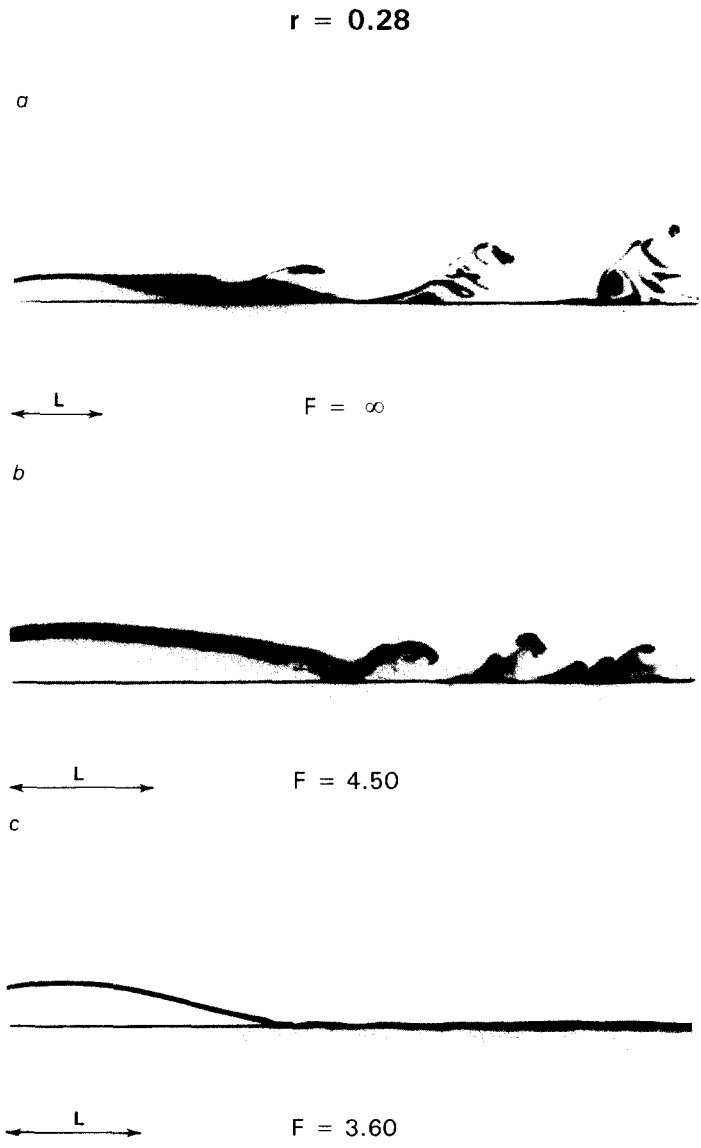

Fig. 5. Fluorescence induced by laser side views for $r = 0.28$ (a) Re = 2950; (b) Re = 4000; (c) Re = 3200; and for $r = 0.8$ (d) Re = 1500; (e) Re = 1800; (f) Re = 1400.

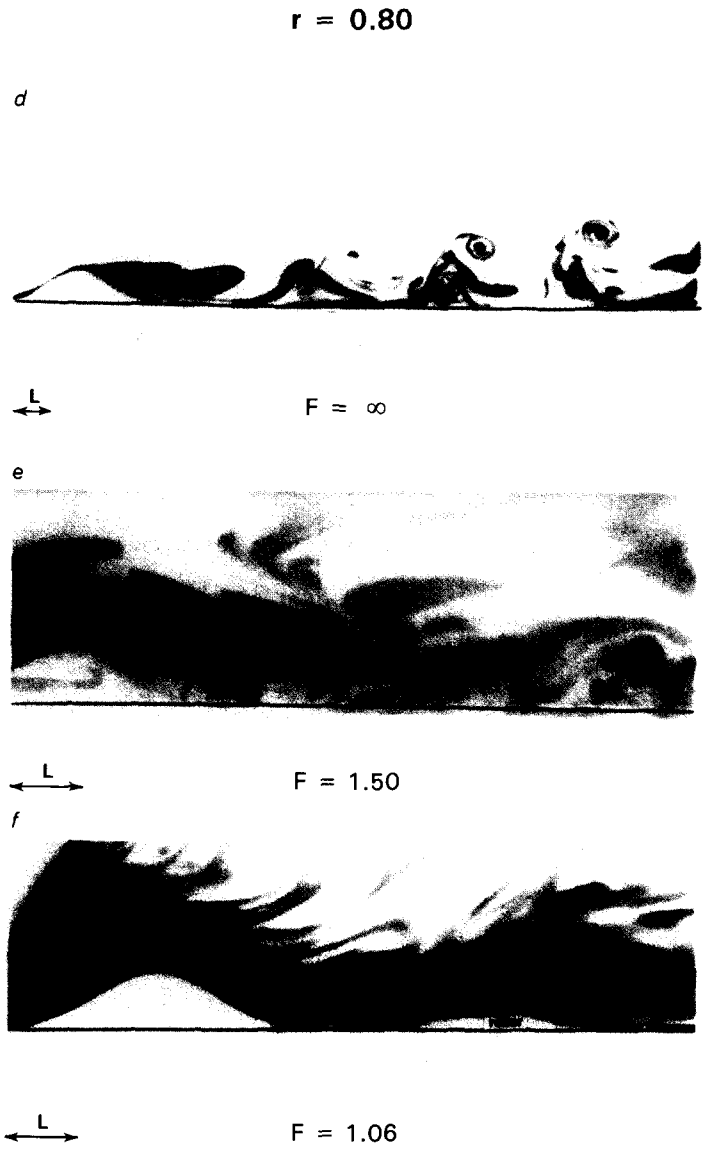

Fig. 5 (continued).

Table 1
Critical Reynolds number, Strouhal and Froude number in function of r

Type	$r = 0.28$	$r = 0.56$	$r = 0.80$	$r = 1.12$
Rec $\pm 10\%$	2000	1200	1300	1000
$S_{vs} \pm 5\%$	0.85	0.55	0.55	0.40
$F_c \pm 5\%$	4.0	2.0	1.2	0.8
$rF_c \pm 5\%$	1.10	1.10	0.96	1.01

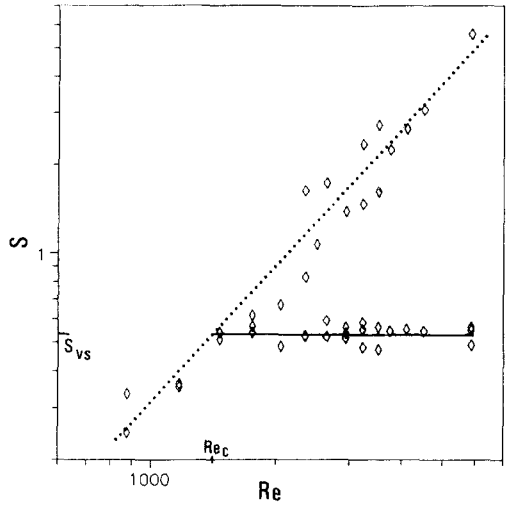

Fig. 6. Evolution of the Strouhal number S versus Re for $r = 0.8$, in the homogeneous case. Dotted line, best power law of the data ($S\mathrm{Re}^{3/2}$).

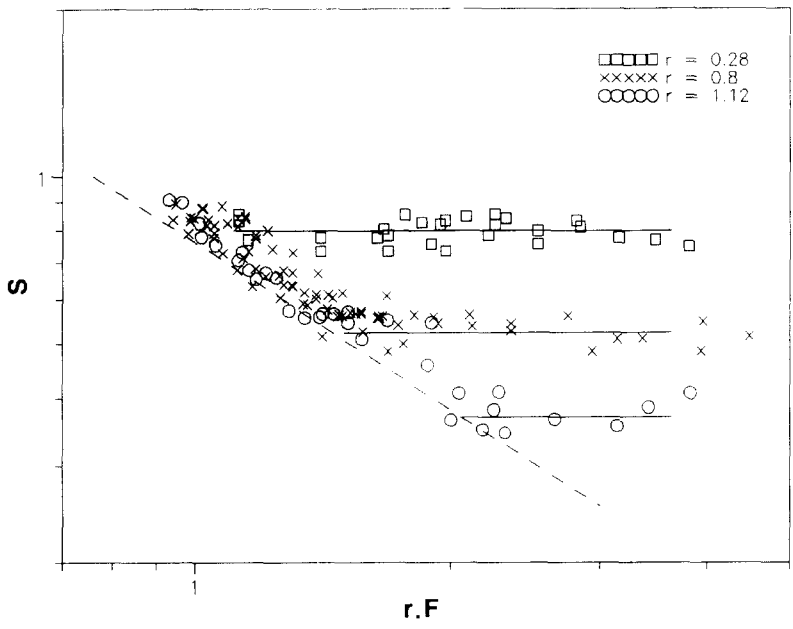

Fig. 7. Strouhal number S of the low-frequency mode for $r = 0.28$ ($750 < \mathrm{Re}(1) < 2000$), $r = 0.8$ ($1000 < \mathrm{Re}(1) < 2900$) and $r = 1.12$ ($2600 < \mathrm{Re}(1) < 4000$).

result demonstrates that the VS mode frequency is controlled by stratification effects until it reaches its asymptotic neutral value. We see also in Fig. 7 and Table 1 that the critical value F_c equals $1/r$ and coincides with the limit of the saturated lee wave regime. The slight scattering, visible in Fig. 7, in the value of S, for given F and r, partly is due to Reynolds number effects, as for each aspect ratio r, up to three different Re(1) have been used. This demonstrates the weak influence of Re as soon as the VS mode is established ($\mathrm{Re} > \mathrm{Re}_c$).

4. The quasi-two-dimensional wake regime

When F decreases below 0.7, the fluid layer that goes around the obstacle, instead of passing over it, starts being animated by quasi-two-dimensional motions.

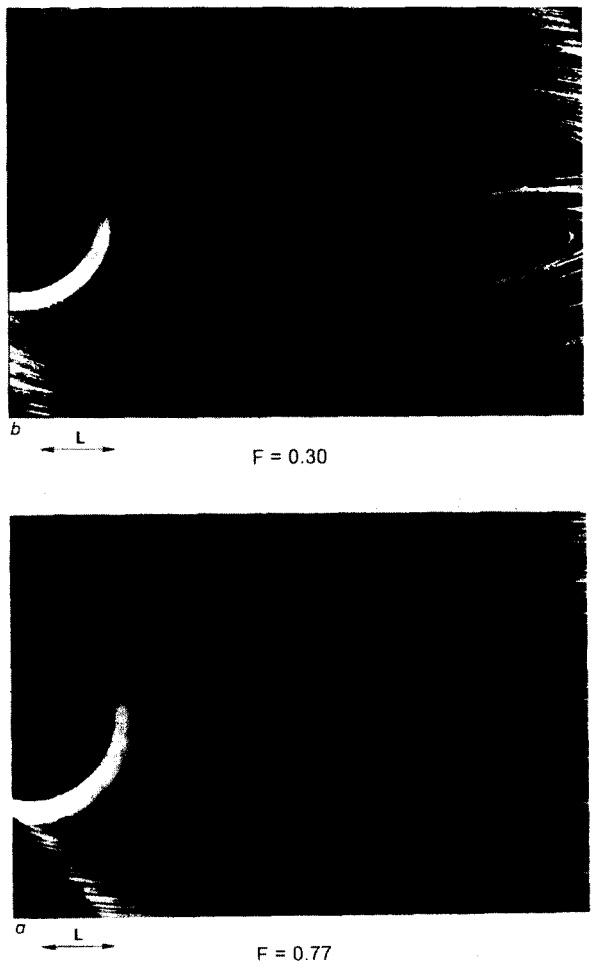

Fig. 8. Particle streak trajectories in a horizontal plane at $z = h/2$, for $r = 0.8$ (Re(1) = 1300). (The flow is from left to right).

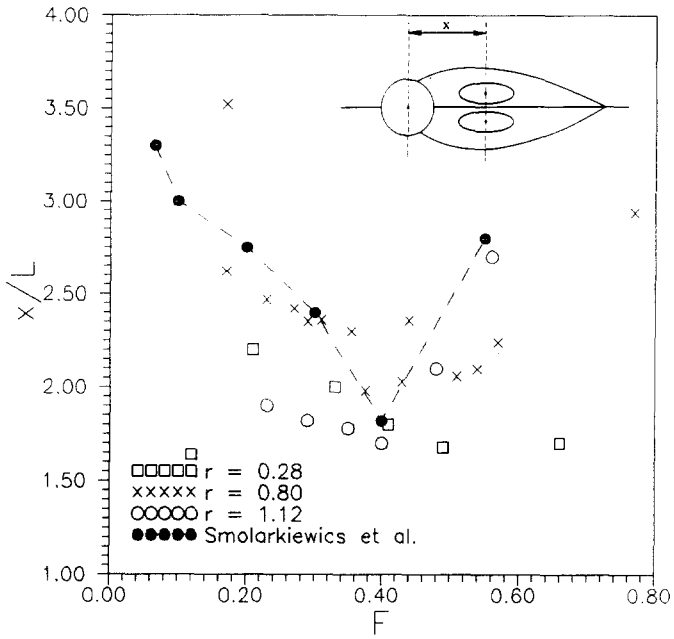

Fig. 9. Evolution versus F of the non-dimensional distance between the centre of vortices and the relief axis.

An attached pair of vortices appears in the lee of the topography (Fig. 8(a)). For the large aspect ratio model ($r = 0.8$), this 2-D layer is topped by a roller visible on the top view of Fig. 8(b) and side view of Fig. 5(f) (roller regime in Fig. 1). This complex structure, described by Sysoeva and Chashechkin (1986) and Chomaz et al. (1993), develops under the first crest of the lee wave and therefore exhibits a similar shape to isophase 2π. For small aspect ratio ($r = 0.28$), rollers are no longer present, probably owing to the rapid drop in the lee wave amplitude with F and also owing to the nearly vertical propagation of the wave energy observed in this case.

Fig. 9 (respectively, Fig. 10) presents measurements of the distance x/L between the centre of the 2-D vortex pair and the centre of the body for $r = 1.12$, $r = 0.8$ and $r = 0.28$ (respectively, the width δ/L). For both the distance x/L and the width δ/L, results are in good agreement with the predictions of Smolarkiewicz and Rotunno (1989) inviscid numerical simulations of the flow over a Witch of Agnesi obstacle. On the contrary, the velocities in the reversed flow region reported by Smolarkiewicz and Rotunno, are approximately five times greater than the experimental ones. This discrepancy certainly is due to the friction at the ground which is not taken into account in the inviscid numerical model. From the relative agreement between the simulations and the present experiments, one is tempted to conclude that the vorticity is mainly generated by the baroclinic

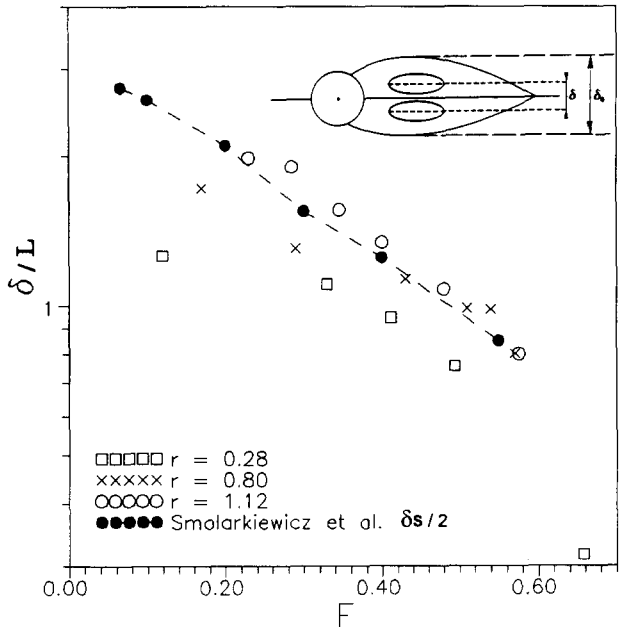

Fig. 10. Evolution versus F of the non-dimensional width between the centre of the vortices. The definition taken here differs from that of Smolarkiewicz and Rotunno by approximately a factor of 2.

mechanism proposed by Smolarkiewicz and Rotunno rather than by separation of the boundary layer on the topography. This issue deserves further investigation.

Acknowledgements

This work was supported by Météo-France. We are grateful to each member of the Simulation Physique des Ecoulements Atmospheriques team from the Centre National de Recherches Météorologiques and to P. Dupont from Institut de Mecanique de Grenoble.

References

Bonneton, P., Chomaz, J.M. and Hopfinger, E.J., 1993. Internal waves produced by the turbulent wake of a sphere moving horizontally in a stratified fluid. J. Fluid Mech., 254: 23–34.

Brighton, P.W.M., 1978. Strongly stratified flow past three-dimensional obstacles. Q. J. R. Meteorol. Soc., 104: 289–307.

Chomaz, J.M., Bonneton, P., Butet, A., Hopfinger, E.J. and Perrier, M., 1992. Froude number dependence of the flow separation line on a sphere towed in a stratified fluid. Phys. Fluids, 4: 254–258.

Chomaz, J.M., Bonneton, P. and Hopfinger, E.J., 1993. The structure of the near wake of a sphere moving horizontally in a stratified fluid. J. Fluid Mech., 254: 1–21.

Crapper, G.D., 1959. A three-dimensional solution for waves in the lee of mountains. J. Fluid Mech., 6: 51–76.

Hunt, J.C.R. and Snyder, W.H., 1980. Experiments on stably and neutrally stratified flow over a model three-dimensional hill. J. Fluid Mech., 96: 671–704.

Kim, H.J. and Durbin, P.A., 1988. Observations of the frequencies in a sphere wake and of drag increase by acoustic excitation. Phys. Fluids, 31: 3260–3265.

Lighthill, M.J., 1978. Waves in Fluids. Cambridge University Press, Cambridge.

Lin, Q., Lindberg, W.R., Boyer, D.L. and Fernando, H.J.S., 1992. Stratified flow past a sphere. J. Fluid Mech., 240: 315–354.

Queney, P., 1948. The problem of the airflow over mountains: a summary of theoretical studies. Bull. Am. Meteorol. Soc., 29: 16–26.

Sheppard, P.A., 1956. Airflow over mountains. Q. J. R. Meteorol. Soc., 82: 528–529.

Smith, R.B., 1980. Linear theory of stratified hydrostatic flow past an isolated mountain. Tellus, 32: 348–364.

Smith, R.B., 1989. Hydrostatic airflow over mountains. Adv. Geophys., 31: 1–41.

Smolarkiewicz, P.K. and Rotunno, R., 1989. Low Froude number flow past three-dimensional obstacles. Part I: Baroclinically generated lee vortices. J. Atmos. Sci., 46: 1154–1164.

Sysoeva, E.Y. and Chashechkin, Y.D., 1986. Vortex structure of a wake behind a sphere in a stratified fluid. J. Appl. Mech. Tech. Phys., 27: 190–196.

Voisin, B., 1994. Internal wave generation in uniformly stratified fluids. Part 2. Moving point sources. J. Fluid Mech., 261: 333–374.